



1 **Interdecadal Pacific Oscillation responsible for the linkage of decadal**  
2 **changes in precipitation/moisture in arid central Asia and humid**  
3 **Asian monsoon region during the last millennium**

4

5 Hongna Xu<sup>1</sup>, Tao Wang<sup>1,2,\*</sup>, Huijun Wang<sup>1,2</sup>

6 <sup>1</sup> Collaborative Innovation Center on Forecast and Evaluation of Meteorological  
7 Disasters (CIC-FEMD), Nanjing University of Information Science and Technology,  
8 Nanjing 210044, China

9 <sup>2</sup> Climate Change Research Center and Nansen-Zhu International Research Centre,  
10 Institute of Atmospheric Physics, Chinese Academy of Sciences, Beijing 100029,  
11 China

12 \* Corresponding author: Tao Wang (wangtao@mail.iap.ac.cn)

13



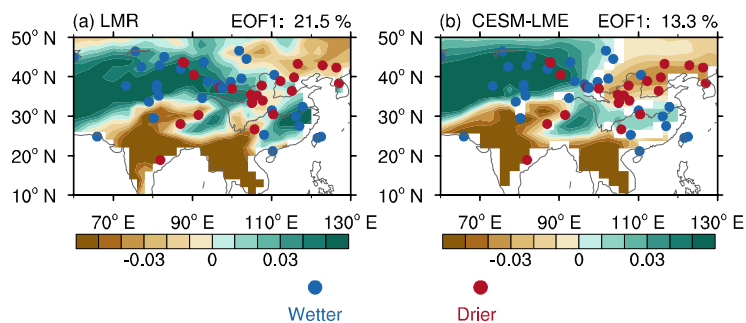
14 **Abstract**

15 Reconstruction and observational studies imply a potential linkage of  
16 moisture/precipitation change in arid central Asia and monsoonal East Asia, in which  
17 the evolution of moisture/precipitation in central Asia is out-of-phase with that in  
18 northern China, but in-phase with that in southern China. In order to ascertain whether  
19 there is a robust linkage between the changes in climate in Asian arid regions and  
20 monsoon regions and to elucidate the underlying dynamic mechanisms, we analyzed  
21 the Last Millennium Reanalysis dataset and output from the Community Earth System  
22 Model-Last Millennium Ensemble (CESM-LME). The results indicate a significant  
23 decadal linkage between precipitation changes in central Asia's arid region and the  
24 Asian monsoon region during the last millennium, which is primarily driven by the  
25 Interdecadal Pacific Oscillation (IPO). In spring, the positive IPO could enhance  
26 westerlies over the Mediterranean Sea and to its east, which could transport more  
27 water vapor and cause increased precipitation over central Asia. In summer, the  
28 positive IPO is accompanied with weakened Asian monsoon and southward Asian  
29 subtropical westerly jet, which can lead to increased (decreased) summer precipitation  
30 over southern China (over northern China and South Asia). The IPO plays a dominant  
31 role in connecting the decadal variations in precipitation between arid central Asia and  
32 monsoonal Asia by modulating the precipitation of their respective major rainy  
33 seasons. Model results suggest that this decadal linkage stems entirely from the  
34 internal variability present in the CESM-LME control and all single-forcing  
35 simulations. Changes in external forcing factors do not alter this inherent linkage



36 caused by IPO. Moreover, based on analyses of the aridity index and soil moisture  
37 content, this relationship of precipitation variation also causes a similar decadal  
38 linkage of moisture changes in central Asia and monsoonal Asia. The differences in  
39 the multi-centennial-scale moisture/precipitation variations in the Asian arid region  
40 and the monsoon region between the Medieval Climate Anomaly and Little Ice Age  
41 are also likely caused by IPO-like sea surface temperature anomalies.

#### 42 Graphical abstract



43

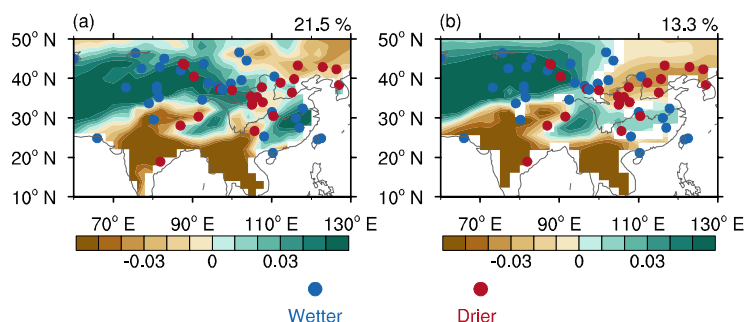
44



## 45 **1 Introduction**

46 The climate of the mid- to low-latitude Asian continent is characterized by an  
47 arid central Asian region and a moist monsoonal region. The climate in central Asia is  
48 mainly controlled by westerlies as a result of its geographical location and blocking  
49 by plateaus and mountains to the southeast (Chen et al., 2010). The main rainy  
50 seasons are spring and winter, especially in southern central Asia (Aizen et al., 2001;  
51 Chen et al., 2011; Xu et al., 2020; Wang et al., 2022). By contrast, the climate in  
52 monsoonal Asia is mainly controlled by the East Asian monsoon and the South Asian  
53 monsoon. The main rainy season is summer as a result of the warm, moist East Asian  
54 summer monsoon (Ding and Chan, 2005) and the South Asian summer monsoon  
55 (Turner and Annamalai, 2012).

56 The Asian arid and monsoonal climates should be independent of each other due  
57 to the dominance of different systems. However, the reconstruction records suggest a  
58 strong linkage between them on a centennial scale. Chen et al. (2015) reviewed  
59 numerous reconstruction studies and indicated that the climate was relatively wetter in  
60 central Asia and southern China, whereas it was relatively drier in northern China  
61 during the Little Ice Age (LIA; 1400–1900 AD) (Fig. 1). During the earlier Medieval  
62 Climate Anomaly (MCA; 1000–1300 AD), the wet and dry changes were the opposite,  
63 with drier conditions in central Asia and southern China and wetter conditions in  
64 northern China.



65

66 **Figure 1.** The reconstructed and simulated first leading precipitation mode. (a) EOF1 of the  
67 nine-year low-pass Lanczos filtered annual precipitation for the time period 850–2000 in the LMR  
68 dataset. The explained variance is given at the top-right. (b) The average EOF1 of the nine-year  
69 low-pass Lanczos filtered annual precipitation in CESM-LME 12 all-forcing simulations for the  
70 time period 850–2005; the shading shows where at least two-thirds of the members agree on the  
71 sign of the average value. The averaged explained variance is given at the top-right. The dots  
72 represent the reconstructed precipitation/moisture records modified from Chen et al. (2015); the  
73 blue (red) dots denote wetter (drier) conditions in the LIA than in the MCA.

74 Clues to the linkage between the climate of the Asian arid regions and the Asian  
75 monsoon regions can also be found based on the limited length of observational data  
76 from the modern era. Since the mid-20th century, the central Asia has become wetter  
77 (Shi et al., 2007; Jiang et al., 2009; Chen et al., 2011; Huang et al., 2013). During the  
78 same period, southern China experienced more precipitation, whereas northern China  
79 received less precipitation and became drier (Ding et al., 2008; Zhao et al., 2010;  
80 Wang et al., 2013). Focusing on two different climatic regions, the precipitation  
81 observations during the period of 1960–2010 also show similar linkage (Huang et al.,  
82 2015). On a decadal scale, central Asia experienced more (less) summer precipitation,  
83 southern China received more (less) summer precipitation, whereas northern China  
84 received less (more) summer precipitation.



85           However, the reconstruction records of the last millennium and the 50-year  
86   observational data only cover less than two periods on the multi-centennial or  
87   interdecadal scale, respectively. It is not sufficient to demonstrate a significant  
88   relationship between the climate of the Asian arid regions and the Asian monsoon  
89   regions. The specific mechanisms behind this possible linkage are still not clear. In  
90   addition, modeling results also indicate that only one out of nine coupled models  
91   within the Paleoclimate Modeling Intercomparison Project Phase 3 (PMIP3) is able to  
92   reproduce the similar climatic linkage between the Asian arid and monsoonal regions  
93   during the MCA and LIA (Shi et al., 2016). Due to the limitations of data length on  
94   the time scales of interest and the large uncertainty in existing model results, therefore,  
95   further research is still needed to confirm whether there is an inherent connection  
96   between the arid regions and monsoon regions in Asia in terms of their dry-wet  
97   variations.

98           In this study, we first focus on the decadal scale and intend to analyze whether  
99   there is a robust linkage between the changes in precipitation pattern in arid regions  
100   and monsoon regions in Asia using the newly released Last Millennium Reanalysis  
101   (LMR) dataset (Tardif et al., 2019; Anderson et al., 2019). Additionally, considering  
102   the superior performance of the Community Earth System Model (CESM) series in  
103   simulating Asian climate (Mishra and Aadhar, 2021; Ning et al., 2020; Xue et al.,  
104   2023), this study will also utilize CESM Last Millennium Ensemble (CESM-LME,  
105   Otto-Bliesner et al., 2016) simulations with multiple samples under different forcing  
106   factors to explore the possible mechanisms underlying the linkage and the potential



107 impacts of different external forcing factors. Thus, the aim of this study is to  
108 investigate the linkage between precipitation/moisture changes in arid central Asia  
109 and monsoonal Asia during the last millennium and its driving factors. The data and  
110 methods used in this study are described in detail in Sect. 2. The linkage between the  
111 changes in precipitation/moisture pattern in arid regions and monsoon regions in Asia  
112 is examined and its driving factors are analyzed in Sect. 3. Finally, the conclusions  
113 and discussion are presented in Sect. 4 and Sect. 5, respectively.

## 114 **2 Data and methods**

### 115 **2.1 Reanalysis data and simulations**

116 In this study, we used the reconstructed annual precipitation anomalies (relative  
117 to the climatological mean of 1951–1980) at a spatial resolution of 2° for the time  
118 period 850–2000 from the LMR Version 2.1 dataset (Tardif et al., 2019; Anderson et  
119 al., 2019) to examine the possible linkage between the Asian arid and monsoonal  
120 regions. The proxy records assimilated in the LMR Version 2.1 dataset are from  
121 PAGES-2k (PAGES2k, 2017). The analyses based on LMR were started with the  
122 “grand mean”, which was an average of 20 LMR reconstructions contained in  
123 aforementioned array. In addition, the reconstructed sea surface temperature (SST)  
124 anomalies from the LMR Version 2.1 dataset are also used to verify the model results.

125 In order to investigate the underlying mechanisms, we analyzed the monthly  
126 outputs of CESM-LME project (Otto-Bliesner et al., 2016). The CESM-LME  
127 simulations are performed using the CESM 1.1 model, in which the atmospheric  
128 component is the Community Atmosphere Model Version 5 (CAM5) (Hurrell et al.,



129 2013). The atmosphere and land (ocean and sea ice) components in the CESM-LME  
130 simulations have the same  $\sim 2^\circ$  ( $\sim 1^\circ$ ) horizontal resolutions as the CESM1.1 model.  
131 We analyzed a total of 35 CESM-LME simulations: one control simulation, 12  
132 all-forcing simulations and 22 single-forcing simulations. The single-forcing  
133 simulations included a subset of five simulations forced by volcanic eruptions, a  
134 subset of four simulations forced by solar activity, a subset of four simulations forced  
135 by ozone and aerosols, three subsets of three simulations forced by greenhouse gases,  
136 land use and land cover, and the Earth's orbit, respectively. The subset of simulations  
137 forced by ozone and aerosols covered the time period 1850–2005, whereas the other  
138 simulations were available for the time period 850–2005. The analyses for the  
139 all-forcing simulations and the six subsets of single-forcing simulations were all based  
140 on the arithmetic mean of multiple members, which was the final step in the analyses.

141 In addition, we also referred to reconstructed moisture/precipitation changes  
142 (relative to the median of entire last millennium) in the LIA and MCA summarized by  
143 Chen et al. (2015). The reconstructions synthesized by Chen et al. (2015) include 71  
144 moisture/precipitation records derived from different types of proxy records (i.e., lake  
145 record, speleothem record, historical documents, tree-ring record, ice-core record,  
146 marine record, peat record, aeolian record, and river terrace). Based on these  
147 moisture/precipitation records, figure 3 in Chen et al. (2015) provided the wetness  
148 grades (i.e., the wetness was classified into dry, moderately dry, moderate, moderately  
149 wet, and wet) for the LIA and MCA at individual sites. The 55 moisture/precipitation  
150 records with different wetness grades between the LIA and MCA were selected in this





151 study to explore the moisture/precipitation changes between these two periods.

## 152 **2.2 Methods**

153 Following Henley et al. (2015), we defined the Interdecadal Pacific Oscillation  
154 (IPO) index as the difference between the SST anomalies averaged over the  
155 central-eastern equatorial Pacific (10 °S–10 °N, 170 °E–90 °W) and the average of the  
156 SST anomalies over the western-central subtropical North Pacific (25–45 °N, 140 °E–  
157 145 °W) and the western-central subtropical South Pacific (50–15 °S, 150 °E–160 °  
158 W). The base period for calculating the IPO index was 1850–1900. To obtain the  
159 filtered version of the index, a nine-year low-pass Lanczos filter was used, coinciding  
160 with the other analyses in this study.

161 We used the aridity index (AI) to quantify the moisture condition of the  
162 terrestrial climate (Middleton and Thomas, 1997):

$$163 \quad AI = \frac{P}{PET} \quad (1)$$

164 where  $P$  is the annual precipitation (units: mm day<sup>-1</sup>), representing the water supply to  
165 land and  $PET$  is the annual potential evapotranspiration (units: mm day<sup>-1</sup>), which  
166 measures the supply of soil water to the atmosphere. A larger aridity index indicates  
167 that relatively more moisture remains in the land, whereas a smaller aridity index  
168 represents drier condition. The outputs of the CESM-LME simulations for soil  
169 moisture (top 10 cm of soil; units: kg m<sup>-2</sup>) were also analyzed to examine the analyses  
170 based on the aridity index. Thus, the analyses related to moisture conditions in this  
171 study were based on both the aridity index and soil moisture content.

172 The Penman–Monteith algorithm (Penman, 1948; Monteith, 1965) is widely



173 used to estimate the potential evapotranspiration and is recommended as a standard  
174 method by the Food and Agriculture Organization of the United Nations (Allen et al.,  
175 1998):

$$176 \quad PET = \frac{0.408\Delta(R_n - G) + \gamma \frac{900}{T_{\text{mean}} + 273} U(e_s - e_a)}{\Delta + \gamma(1 + 0.34U)} \quad (2)$$

177 where the  $R_n$  is the net surface radiation (units:  $\text{MJ m}^{-2} \text{ day}^{-1}$ ), the  $G$  is soil heat flux  
178 density (units:  $\text{MJ m}^{-2} \text{ day}^{-1}$ ); the difference between them represents the available  
179 energy.  $\gamma$  is the psychrometric constant (units:  $\text{kPa } ^\circ\text{C}^{-1}$ ),  $T_{\text{mean}}$  is the mean  
180 temperature (units:  $^\circ\text{C}$ ; i.e., the average of the 2-m daily maximum and daily  
181 minimum air temperatures);  $\Delta$  is the slope vapor pressure curve (units:  $\text{kPa } ^\circ\text{C}^{-1}$ )  
182 derived from  $T_{\text{mean}}$ ,  $U$  is the 2-m wind speed (units:  $\text{m s}^{-1}$ );  $e_s$  is the saturation vapor  
183 pressure (units:  $\text{kPa}$ ), derived from the daily maximum and daily minimum air  
184 temperatures;  $e_a$  is the actual vapor pressure (units:  $\text{kPa}$ ), calculated from  $e_s$  and the  
185 relative humidity.

186 Empirical orthogonal function (EOF) analysis was performed on the  
187 standardized annual precipitation to identify the first leading precipitation mode over  
188 the Asian continent. A nine-year low-pass Lanczos filter was applied to the  
189 standardized precipitation before EOF analysis to remove the variability on  
190 interannual and shorter timescales. The same analyses were also applied to the aridity  
191 index and the annual soil moisture content to obtain the first leading decadal moisture  
192 mode over the Asian continent. Linear regression analyses were applied to understand  
193 the root cause of the leading decadal precipitation/moisture modes and their statistical  
194 significance was examined by a two-sided  $t$ -test. Because of the low-pass Lanczos



195 filter before linear regression analyses, the effective degree of freedom  $N^*$  in the  $t$ -test  
196 was calculated following Bretherton et al. (1999):

$$197 \quad N^* = N \frac{1-r_a r_b}{1+r_a r_b} \quad (3)$$

198 where  $r_a$  ( $r_b$ ) is the autocorrelation at lag 1 for variables  $a$  ( $b$ ) and  $N$  is the original  
199 length of the time series. A two-sided  $t$ -test was also applied to examine the statistical  
200 significance of climate changes between the LIA and the MCA. Besides, the  
201 consistency of results derived from multiple members (i.e., analyses based on  
202 all-forcing simulations and the six subsets of single-forcing simulations) was  
203 examined by counting the percentage of members whose results' signs are the same as  
204 the arithmetic mean of multiple members. A power spectrum analysis was performed  
205 on the time series of the leading precipitation mode and the IPO index to obtain their  
206 dominant periodicity, the statistical significance of which was examined via the power  
207 spectrum of the mean red noise (Gilman et al., 1963).

208 In this study, winter, spring, summer, and autumn were defined as December–  
209 February, March–May, June–August, and September–November, respectively.

### 210 **3 Results**

#### 211 **3.1 Reconstructed and simulated first leading precipitation mode**

212 Based on the LMR data, the first leading mode (EOF1) of the decadal changes in  
213 Asian precipitation in the last millennium showed the same changes in precipitation in  
214 arid central Asia and southern China, which were the opposite of those in the South  
215 Asian monsoon region (including the southern Tibetan Plateau, the Indian Peninsula  
216 and the Indo-China Peninsula) and most of northern China (Fig. 1a). This mode



217 accounted for 21.5% of the total variance of precipitation in Asia in the last  
218 millennium.

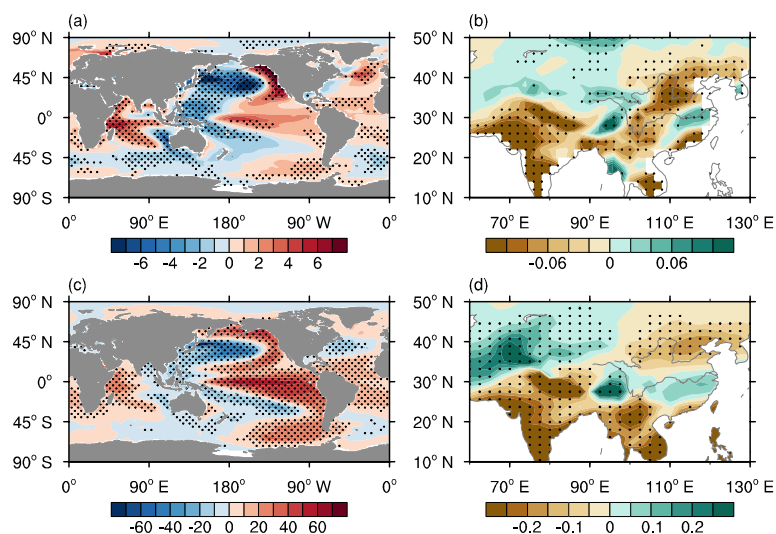
219 We also analyzed the outputs of the CESM-LME simulations. In the all-forcing  
220 simulations, most members reproduced similar first leading precipitation mode with  
221 the reconstruction for the time period 850–2005 (Fig. S1). Their ensemble pattern was  
222 also consistent with the reconstruction (Fig. 1b). The averaged explained variance was  
223 13.3% (ranging from 11.7 to 14.8%). These same patterns of changes in precipitation  
224 between the long-term simulations and the reconstruction suggest that, on the decadal  
225 scale, there is a robust linkage between the changes in precipitation pattern in arid  
226 regions and monsoon regions. This decadal linkage suggests that the evolution of  
227 precipitation in central Asia is out-of-phase with that in northern China and South  
228 Asian monsoon region, but in-phase with that in southern China. The linkage between  
229 the arid central Asian region and the East Asian monsoon region is consistent with the  
230 relationship of changes in precipitation based on observational data for the last 60  
231 years (Huang et al., 2015). Our analysis suggests that this observed relationship has  
232 persisted over the last millennium. Our results also indicated that the decadal changes  
233 in precipitation in the South Asian monsoon region are also closely related to the  
234 changes in the arid central Asian region and the East Asian monsoon region.

### 235 **3.2 Dominant role of the IPO**

236 Many studies have shown that the SST anomaly is an important factor in  
237 modulating the decadal variability in precipitation over Asia (e.g., Chu et al., 2018;  
238 Huang et al., 2019). We therefore calculated the linear regression of the SST onto the



239 time series of the leading precipitation mode. Figure 2a and 2c show that higher  
240 (lower) SSTs appeared over the central-eastern equatorial Pacific (the western-central  
241 parts of both the subtropical North Pacific and South Pacific) in the LMR and  
242 all-forcing simulations. The Pacific basin-wide SST anomalies resembled the positive  
243 pattern of the IPO (Power et al., 1999; Henley et al., 2015; Wang and Miao, 2018).  
244 The precipitation anomalies during the positive phases of the IPO showed positive  
245 anomalies in arid central Asia and southern China and negative anomalies in the  
246 South Asian monsoon region and most of northern China (Fig. 2b and 2d), resembling  
247 the leading decadal precipitation mode in the LMR and all-forcing simulations. It is  
248 therefore likely that the IPO dominated the decadal linkage between the changes in  
249 precipitation pattern in arid regions and monsoon regions in Asia.



250  
251 **Figure 2.** The dominant role of the IPO. The reconstructed (a) annual SST anomalies (units: °C)  
252 regressed onto the time series of the leading decadal precipitation mode and (b) annual  
253 precipitation anomalies (units: mm day<sup>-1</sup>) regressed onto the time series of the IPO index in the  
254 Last Millennium Reanalysis dataset. The dots in parts (a, b) show significant anomalies at the 95%



255 confidence level. (c) Annual SST anomalies (units: °C) regressed onto time series of the leading  
256 decadal precipitation mode and (d) annual precipitation anomalies (units: mm day<sup>-1</sup>) regressed  
257 onto the time series of the IPO index simulated by multiple members of the CESM-LME  
258 all-forcing runs. Dots in parts (c, d) show that the significant anomalies at the 95% confidence  
259 level simulated by at least two-thirds of the members agree on the sign of the average of multiple  
260 members.

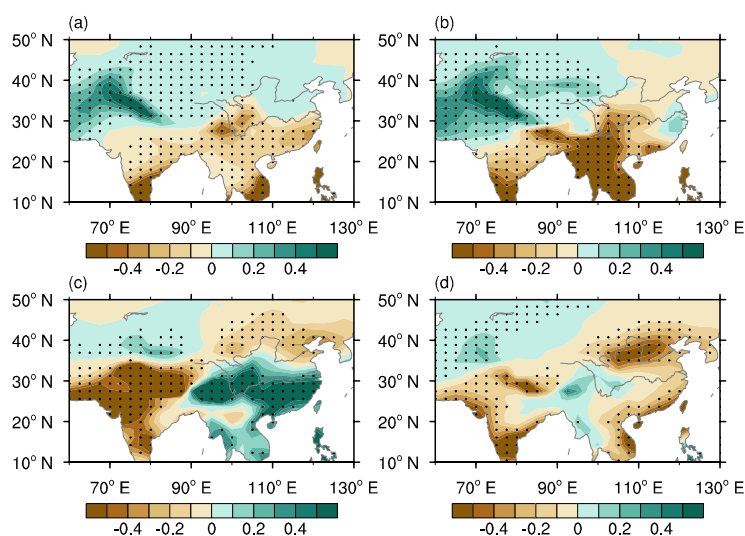
261 We applied power spectrum analysis to explore the temporal characteristics of  
262 the first leading precipitation mode and the IPO. Both the leading precipitation mode  
263 and the IPO had a common frequency band of 10–20 years in the LMR and  
264 all-forcing simulations (Figs. S2–4), indicating that the IPO dominated the linkage  
265 between the changes in precipitation pattern in arid regions and monsoon regions in  
266 Asia at decadal to bi-decadal scales during the last millennium. The consistency  
267 between the reconstruction and the simulations indicates the reliability of the  
268 simulations, which is the foundation of the following analyses on the relevant  
269 mechanism based on simulations.

### 270 **3.3 Processes of the IPO modulating the leading precipitation pattern**

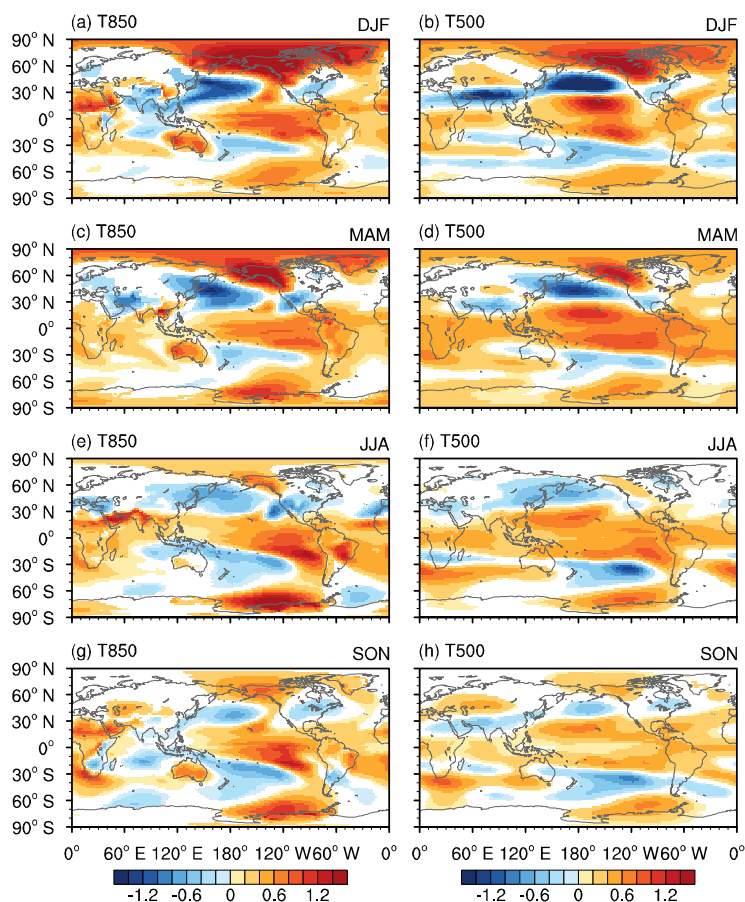
271 Because there is a seasonal cycle in precipitation and the atmospheric circulation  
272 over Asia, especially over monsoonal Asia, we analyzed the seasonal changes in  
273 precipitation associated with the IPO. During the positive phases of IPO, in the arid  
274 central Asia, the precipitation in the four seasons all increased and made a positive  
275 contribution to the increase in annual precipitation (Fig. 3). The precipitation  
276 anomalies were larger in spring and winter, especially in spring, in which season the  
277 precipitation accounted for the most of the annual precipitation (Fig. S5). The largest



278 increase in spring precipitation was mainly in southern central Asia. In East Asia,  
279 summer precipitation increased (decreased) over southern (northern) China and  
280 autumn precipitation decreased over northern China, both contributing positively to  
281 the annual changes in precipitation. By contrast, spring and winter precipitation both  
282 decreased over southern China, partly offsetting the positive contribution of summer  
283 precipitation to the increase in annual precipitation in this region. Precipitation in all  
284 four seasons decreased in most of the South Asian monsoon regions, contributing  
285 positively to the decrease in annual precipitation. Then, we analyzed the seasonal  
286 atmospheric circulation anomalies associated with the IPO to determine the processes  
287 by which the IPO modulated these seasonal changes in precipitation.



288  
289 **Figure 3.** Simulated seasonal precipitation anomalies during the positive phases of the IPO.  
290 Regressed maps of (a) winter, (b) spring, (c) summer, and (d) autumn precipitation anomalies  
291 (units:  $\text{mm day}^{-1}$ ) onto the time series of the IPO index simulated by multiple members of the  
292 CESM-LME all-forcing runs. Dots show that the significant anomalies at the 95% confidence  
293 level simulated by at least two-thirds of the members agree on the sign of the average of multiple  
294 members.



295

296 **Figure 4.** Simulated seasonal temperature anomalies during the positive phases of the IPO.  
297 Regressed maps of 850 hPa temperature anomalies (units: °C) in (a) winter, (c) spring, (e) summer,  
298 and (g) autumn onto the time series of the IPO index simulated by multiple members of the  
299 CESM-LME all-forcing runs. (b) Winter, (d) spring, (f) summer, and (h) autumn for 500 hPa  
300 temperature anomalies (units: °C). Shading shows that the significant anomalies at the 95%  
301 confidence level simulated by at least two-thirds of the members agree on the sign of the average  
302 of multiple members.

303 In spring, warming appeared over the northern low and high latitudes, whereas  
304 cooling appeared over the northern mid-latitudes, especially in the eastern hemisphere,  
305 corresponding to a positive phase of the IPO (Fig. 4c and 4d). The tropospheric



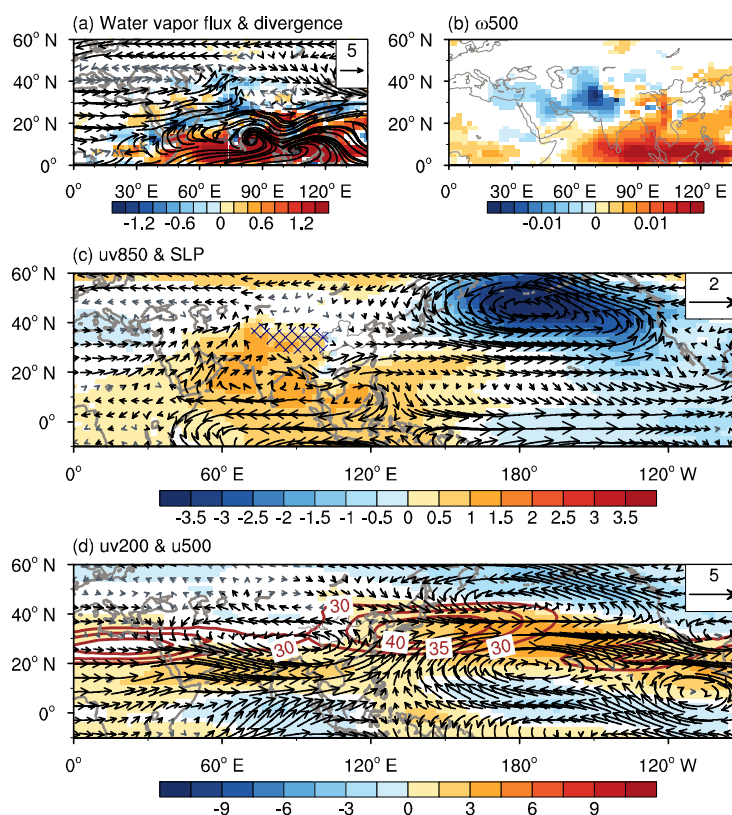


306 temperature anomalies led to an enhanced (weakened) meridional temperature  
307 gradient over low (high) latitudes as the climatological temperature decreased from  
308 low to high latitudes. The anomalies in the temperature gradient contributed to  
309 enhanced westerlies over low latitudes and weakened westerlies over high latitudes  
310 via the thermal wind relation (Fig. 5c and 5d), indicating a southward shift of the  
311 mid-latitude westerlies. The enhanced westerlies over the Mediterranean Sea and to  
312 its east transported more water vapor from the Mediterranean Sea to southern central  
313 Asia (Fig. 5a).

314 Positive sea-level pressure (SLP) anomalies appeared over the Indo–western  
315 Pacific warm pool and negative SLP anomalies appeared over the eastern tropical  
316 Pacific (Fig. 5c), consistent with the SST anomalies during positive IPO phases. The  
317 distribution of the SLP anomalies indicated a weakened Walker circulation over the  
318 Pacific Ocean, which further led to suppressed convection over the maritime continent  
319 (Li et al., 2022). The decreased latent heating associated with the decreased  
320 precipitation over the maritime continent can produce westward-propagating  
321 baroclinic Rossby wave trains (Jiang et al., 2021). This resulted in anomalous  
322 low-level anticyclone and upper-level cyclone over the Indian subcontinent, both of  
323 which led to anomalous southerlies over central Asia (Fig. 5c and 5d). The anomalous  
324 southerlies induced warm advection and led to anomalous ascending motion in this  
325 region (Fig. 5b). In addition, the anomalous southerlies at low troposphere also could  
326 transport more water vapor from low latitudes to central Asia (Fig. 5a). The enhanced  
327 transport of water vapor and the anomalous ascending motion both favored increased



328 precipitation in spring over central Asia. In summary, the IPO affected the  
329 precipitation from westerly winds through modulating the mid-latitude westerlies and  
330 the Walker circulation in the Pacific Ocean.



331  
332 **Figure 5.** Simulated spring atmospheric circulation anomalies during the positive phases of the  
333 IPO. Regressed maps of anomalous (a) vertically integrated water vapor flux from 1000 to 300  
334 hPa (vectors; units:  $\text{kg m}^{-1} \text{s}^{-1}$ ) and its divergence (shading; units:  $10^{-5} \text{kg m}^{-2} \text{s}^{-1}$ ), (b) 500 hPa  
335 vertical velocity ( $\omega_{500}$ ) (units:  $\text{Pa s}^{-1}$ ), (c) 850 hPa wind (uv850) (vectors; units:  $\text{m s}^{-1}$ ) and SLP  
336 (shading; units: hPa), (d) 200 hPa wind (uv200) (vectors; units:  $\text{m s}^{-1}$ ) and 500 hPa zonal wind  
337 (u500) (shading; units:  $\text{m s}^{-1}$ ) onto the time series of the IPO index simulated by the CESM-LME  
338 all-forcing runs. The blue hatched patterns in part (c) indicate the region with an altitude  $>3000$  m.  
339 The brown contours in part (d) are the climatological 200 hPa zonal wind (units:  $\text{m s}^{-1}$ ). The  
340 shading shows that the significant anomalies at the 95% confidence level simulated by at least  
341 two-thirds of the members agree on the sign of the average. The black vectors show that the



342 significant anomalies at the 95% confidence level simulated by at least two-thirds of the members  
343 agree on the sign of the average for the zonal or meridional component.

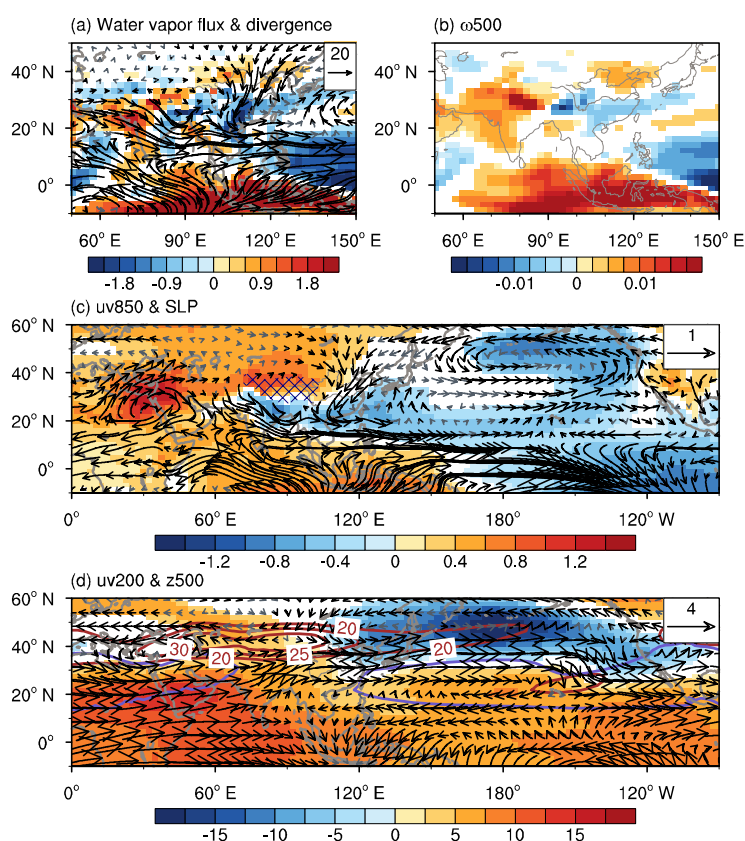
344 The circulation anomalies associated with the IPO in winter were similar to those  
345 in spring (Fig. S6), indicating that the processes by which the IPO modulated winter  
346 precipitation in central Asia were similar to those in spring.

347 In summer, higher (lower) SLPs appeared over the most of the Asian continent  
348 (northern Pacific) during the positive phases of the IPO (Fig. 6c). This was the reverse  
349 of the climatological state, in which the SLP over most of the Asian continent was  
350 lower than that over the neighboring oceans. A weakened land–sea thermal contrast  
351 was therefore induced. The weakened land–sea thermal contrast led to a weakened  
352 Asian summer monsoon (ASM), featured by northerly anomalies at 850 hPa over the  
353 whole of monsoonal Asia (Fig. 6c). The northerly anomalies further led to weakened  
354 water vapor transport in this region (Fig. 6a).

355 Anomalies also appeared in the tropospheric temperature (Fig. 4e and 4f) and  
356 caused westerly (easterly) anomalies over the south (north) of the climatological  
357 Asian subtropical westerly jet at 200 hPa (Fig. 6d). The wind anomalies indicated the  
358 southward shift in the Asian subtropical westerly jet and the associated secondary  
359 meridional–vertical circulation (Cressman, 1981; Ding, 2005; Zhang and Huang,  
360 2011), which led to anomalous downward motion over northern China and anomalous  
361 upward motion over southern China (Fig. 6b) (Wang et al., 2013; Zhu et al., 2015).  
362 The western Pacific subtropical high shifted southeastward (Fig. 6d), which did not  
363 favor the transport of water vapor to northern China (Fig. 6a). These circulation



364 anomalies all indicate a weakened ASM system (Webster and Yang, 1992; Wang,  
365 2001). Precipitation over southern China therefore increased in summer, whereas  
366 precipitation over northern China and most of the South Asian monsoon regions  
367 decreased. In summary, the IPO affected the monsoon precipitation through  
368 modulating the ASM system.



369  
370 **Figure 6.** Simulated summer atmospheric circulation anomalies during the positive phases of the  
371 IPO. Regressed maps of anomalous (a) vertically integrated water vapor flux from 1000 to 300  
372 hPa (vectors; units:  $\text{kg m}^{-1} \text{s}^{-1}$ ) and its divergence (shading; units:  $10^{-5} \text{kg m}^{-2} \text{s}^{-1}$ ), (b) 500 hPa  
373 vertical velocity ( $\omega_{500}$ ) (units:  $\text{Pa s}^{-1}$ ), (c) 850 hPa wind (uv850) (vectors; units:  $\text{m s}^{-1}$ ) and SLP  
374 (shading; units: hPa), and (d) 200 hPa wind (uv200) (vectors; units:  $\text{m s}^{-1}$ ) and 500 hPa  
375 geopotential height (z500) (shading; units: m) onto the time series of the IPO index simulated by



376 the CESM-LME all-forcing runs. The blue hatched patterns in part (c) indicate the region with an  
377 altitude >3000 m. The brown contours in part (d) are the climatological 200 hPa zonal wind (units:  
378  $\text{m s}^{-1}$ ). The purple line in part (d) is the isoline with a value of 5860 m in the climatology state.  
379 The shading shows that the significant anomalies at the 95% confidence level simulated by at least  
380 two-thirds of the members agree on the sign of the average. The black vectors show that the  
381 significant anomalies at the 95% confidence level simulated by at least two-thirds of the members  
382 agree on the sign of the average for the zonal or meridional component.

383 In autumn, negative anomalies in the 500 hPa geopotential height appeared over  
384 the Korean Peninsula (Fig. S7d), indicating a strengthened East Asian trough (EAT)  
385 during the positive phases of the IPO (Qin et al., 2018, 2020; Li et al., 2020). The  
386 strengthened EAT contributed to northerly anomalies over East Asia (Fig. S7c), which  
387 led to weakened water vapor transport in this region (Fig. S7a). The anomalous  
388 northerlies to the west of the strengthened EAT induced cold advection (Fig. S7c and  
389 S7d) and led to anomalous descending motion over northern China (Fig. S7b).  
390 Precipitation therefore decreased over northern China in autumn.

391 Consistent with the SST anomalies during the positive phases of the IPO,  
392 positive (negative) SLP anomalies appeared over the Indo–western Pacific warm pool  
393 (eastern tropical Pacific) in all four seasons (Figs. 5c, 6c, S6c and S7c), indicating a  
394 weakened Walker circulation in the Pacific Ocean, which is in agreement with the  
395 results in Dong and Lu (2013) and Zhao et al. (2021). This weakened Walker  
396 circulation contributed to decreased precipitation over most of the South Asian  
397 monsoon regions (Krishnamurthy and Krishnamurthy, 2014; Li et al., 2021).

### 398 **3.4 Decisive role of internal variability**

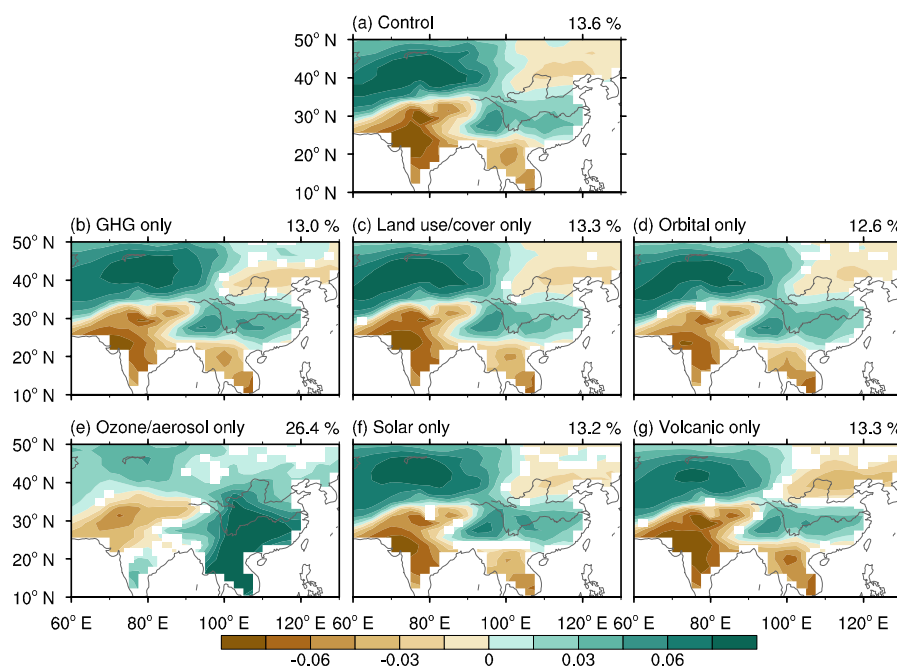
399 Many studies have suggested that both external forcings and internal variability



400 could affect the decadal variability of precipitation over Asia (e.g., Wang et al., 2013;  
401 Jin et al., 2019; Zhu et al., 2022). To identify the roles of internal variability and  
402 external forcing, Fig. 7 shows the first leading decadal precipitation modes of the  
403 control and single-forcing simulations. The decadal linkage between the changes in  
404 precipitation pattern in central Asia and monsoonal Asia in the all-forcing simulations  
405 also appeared in the control simulation (Fig. 7a), implying this decadal linkage was  
406 mainly caused by the internal variability. Nearly all the single-forcing simulations  
407 presented similar decadal linkage with all-forcing simulations, apart from the  
408 simulations forced by ozone and aerosols (Fig. 7b–g). This indicated that, during the  
409 last millennium, volcanic eruptions, solar activity, greenhouse gases, land use and  
410 land cover, and the Earth’s orbit were unable to change the decadal linkage between  
411 the changes in precipitation pattern in arid regions and monsoon regions in Asia,  
412 which was dominated by the internal variability. Only in the ozone and aerosols  
413 forcing simulations, which covered the period of 1850–2005, the decadal linkage of  
414 precipitation changes disappeared. We further examined the results of other forcing  
415 simulations for the period of 1850–2005 (Fig. S8), and all the first decadal  
416 precipitation modes simulated by other forcing experiments still indicated similar  
417 decadal linkage with all-forcing last-millennium simulations. This meant that since  
418 the industrial revolution, only the ozone and aerosol forcing factors can change the  
419 dominant mode of the reverse variation of precipitation in East Asia from north to  
420 south and present stronger local climate effects. As noted by Wang et al. (2013), it  
421 may be that anthropogenic aerosols play a more important role in regulating



422 precipitation in East Asia, which needs further analysis.



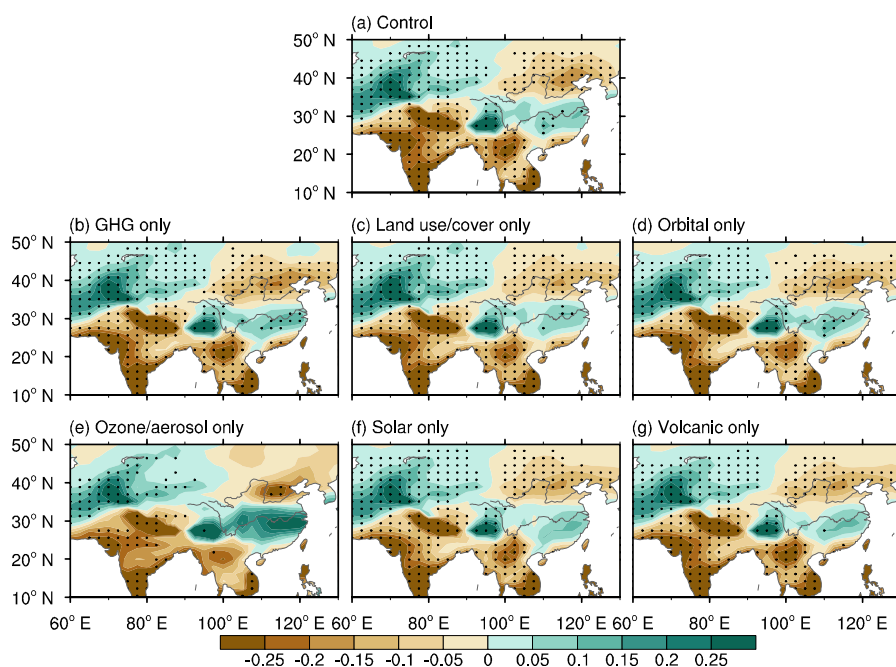
423

424 **Figure 7.** The leading decadal precipitation mode for the time period 850–2005 in the control and  
425 single-forcing simulations. **(a)** EOF1 of the nine-year low-pass Lanczos filtered annual  
426 precipitation in the control simulation. The explained variance is given at the top-right. **(b–g)** The  
427 average EOF1 of the nine-year low-pass Lanczos filtered annual precipitation in six subsets of the  
428 single-forcing simulations: a subset of three simulations forced by greenhouse gas emissions  
429 (GHG); a subset of three simulations forced by land use and land cover; a subset of three  
430 simulations forced by the Earth’s orbit; a subset of four simulations forced by ozone and aerosols;  
431 a subset of four simulations forced by solar activity; and a subset of five simulations forced by  
432 volcanic eruptions. The averaged explained variance is given at the top-right. The shading in parts  
433 **(b–g)** shows where at least two-thirds of the members agree on the sign of the average of multiple  
434 members.

435 Apart from the simulations forced by ozone and aerosols, the SST anomalies  
436 associated with the leading precipitation mode in the control and single-forcing  
437 simulations all showed a positive IPO pattern (Fig. S9), consistent with the all-forcing



438 simulations. At the same time, the precipitation anomalies associated with the positive  
439 IPO in the control and single-forcing simulations all showed positive anomalies in  
440 arid central Asia and southern China and negative anomalies in the South Asian  
441 monsoon region and most of northern China (Fig. 8), also consistent with the  
442 all-forcing simulations. This suggested that these external forcing factors cannot  
443 change the dominant influence of IPO on Asian decadal precipitation and lead to the  
444 decadal linkage between the changes in precipitation pattern in arid regions and  
445 monsoon regions in Asia during the last millennium. It is therefore clear that the  
446 internal variability associated with the IPO had a decisive role in shaping the decadal  
447 linkage of precipitation changes.



448  
449 **Figure 8.** Simulated precipitation anomalies during the positive phases of the IPO in the control  
450 and single-forcing simulations. **(a)** Precipitation anomalies (units:  $\text{mm day}^{-1}$ ) regressed onto the  
451 time series of the IPO index in the control run. The dots show significant anomalies at the 95%





452 confidence level. **(b–g)** Precipitation anomalies (units:  $\text{mm day}^{-1}$ ) regressed onto the time series of  
453 the IPO index in six subsets of the single-forcing simulations. The dots show that the significant  
454 anomalies at the 95% confidence level simulated by at least two-thirds of the members agree on  
455 the sign of the average of multiple members.

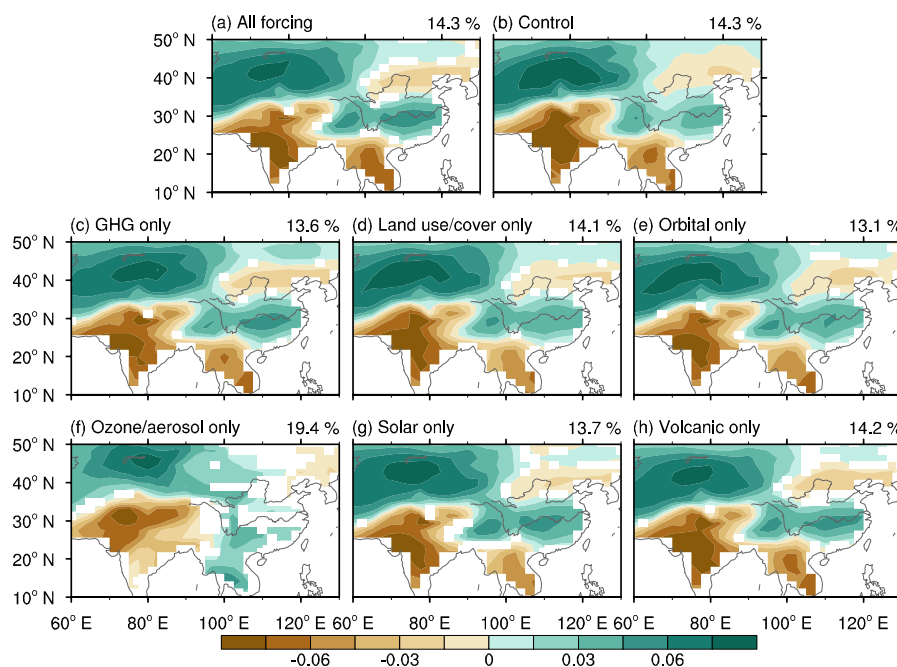
456 In the ozone and aerosols forcing simulations, we can find positive precipitation  
457 anomalies in arid central Asia and southern China and negative precipitation  
458 anomalies in the South Asian monsoon region and most of northern China during the  
459 positive phases of the IPO (Fig. 8e). However, the changes in East Asian precipitation  
460 were no longer significant, which meant that the impacts of IPO on East Asian  
461 precipitation in this experiment were weakened.

### 462 **3.5 Simulated first leading moisture mode**

463 Terrestrial moisture conditions are closely related to precipitation changes and  
464 could strongly affect terrestrial ecosystems. The terrestrial moisture condition is  
465 quantified by both aridity index and soil moisture content here. Based on our analyses  
466 of the aridity index (Fig. 9a) and the soil moisture content (Fig. S10a), we found that  
467 the EOF1 of the decadal changes in Asian moisture during the last millennium also  
468 showed the same changes in moisture in arid central Asia and southern China, which  
469 were the opposite of those in the South Asian monsoon region and most of northern  
470 China. This is consistent with the first leading precipitation mode, suggesting the  
471 important contribution of precipitation to the decadal linkage between the changes in  
472 moisture pattern in arid regions and monsoon regions in Asia. Similar first leading  
473 moisture mode was seen in all the experiments apart from those with only ozone and  
474 aerosol forcing (Figs. 9 and S10), indicating the decisive role of internal variability on



475 the decadal linkage of moisture changes.



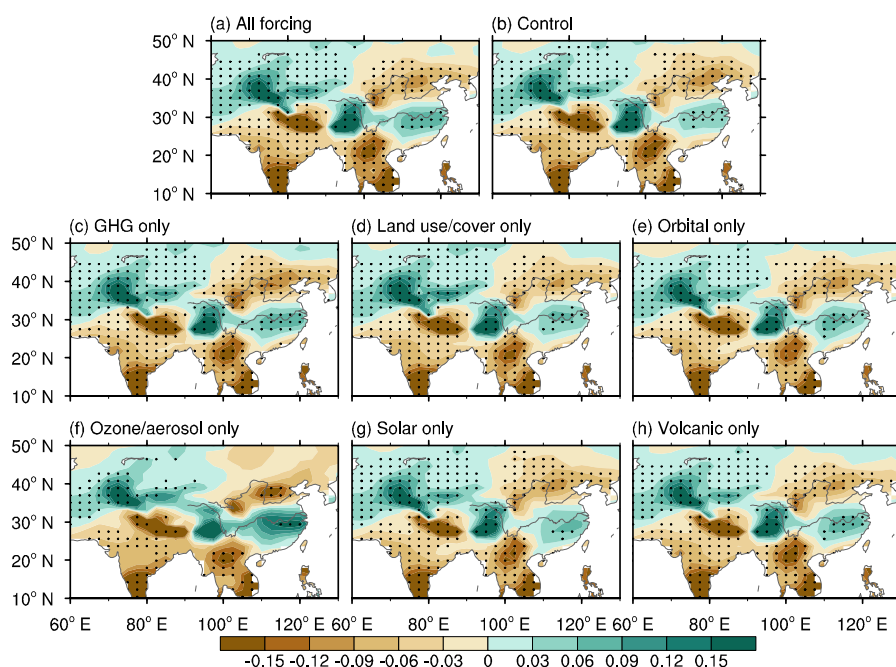
476

477 **Figure 9.** The simulated leading decadal aridity index mode for the time period 850–2005. **(a)** The  
478 average EOF1 of the nine-year low-pass Lanczos filtered aridity index in the all-forcing  
479 simulations. The averaged explained variance is given at the top-right. **(b)** EOF1 of the nine-year  
480 low-pass Lanczos filtered aridity index in the control simulation. The explained variance is given  
481 at the top-right. **(c–h)** The average EOF1 of the nine-year low-pass Lanczos filtered aridity index  
482 in six subsets of the single-forcing simulations. The averaged explained variance is given at the  
483 top-right. The shading in parts **(a, c–h)** shows where at least two-thirds of the members agree on  
484 the sign of the average of multiple members.

485 The SST anomalies associated with the leading moisture mode in all experiments,  
486 apart from those with only ozone and aerosol forcing, showed a positive IPO pattern  
487 (Figs. S11 and S12), indicating the dominant role of the IPO on the decadal linkage of  
488 moisture changes. The moisture anomalies associated with the positive IPO showed  
489 positive anomalies in arid central Asia and southern China and negative anomalies in



490 the South Asian monsoon region and most of northern China in all the experiments  
491 (Figs. 10 and S13), consistent with the leading moisture mode. This further confirmed  
492 the abovementioned dominant role of the IPO. Therefore, the internal variability  
493 associated with the IPO also had a decisive role in shaping the decadal linkage  
494 between the changes in moisture pattern in arid regions and monsoon regions in Asia  
495 through regulating precipitation during the last millennium.



496  
497 **Figure 10.** Simulated aridity index anomalies during the positive phases of the IPO. The aridity  
498 index anomalies regressed onto the time series of the IPO index in the (a) all-forcing simulations,  
499 (b) control simulation, and (c–h) six subsets of the single-forcing simulations. The dots in part (b)  
500 show significant anomalies at the 95% confidence level and the dots in parts (a, c–h) denote that  
501 the significant anomalies at the 95% confidence level simulated by at least two-thirds of the  
502 members agree on the sign of the average value.

#### 503 4 Conclusions

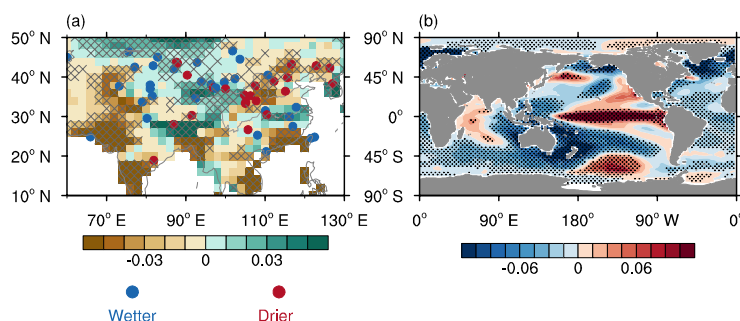


504           Based on the LMR dataset and CESM-LME all-forcing simulations, the first  
505 leading precipitation mode in Asia on decadal scale during the last millennium  
506 showed the same changes in precipitation in arid central Asia and southern China,  
507 which were the opposite of those in the South Asian monsoon region and most of  
508 northern China. This mode indicated a robust linkage between the changes in  
509 precipitation pattern in arid regions and monsoon regions in Asia on decadal scale, in  
510 which the evolution of precipitation in central Asia was out-of-phase with that of  
511 northern China and the South Asian monsoon regions and in-phase with that of  
512 southern China.

513           Further analysis based on CESM-LME all-forcing, control and all single-forcing  
514 simulations showed that the internal variability associated with the IPO plays a  
515 dominant role in connecting the decadal variations in precipitation between arid  
516 central Asia and monsoonal Asia by modulating the precipitation of their respective  
517 major rainy seasons during the last millennium. In spring, the positive IPO could  
518 enhance westerlies over the Mediterranean Sea and to its east, which could transport  
519 more water vapor and cause increased precipitation over central Asia. In summer, the  
520 positive IPO is accompanied with weakened Asian summer monsoon and southward  
521 Asian subtropical westerly jet, which further lead to increased (decreased) summer  
522 precipitation over southern China (over northern China and South Asian monsoon  
523 region). Besides, the positive IPO can weaken Pacific Walker circulation, which  
524 contributes to precipitation decrease over South Asian monsoon regions in all four  
525 seasons.



526 In addition, this decadal linkage of precipitation variation also causes a similar  
527 decadal linkage of moisture changes in central Asia and monsoonal Asia during the  
528 last millennium.



529  
530 **Figure 11.** Reconstructed changes in (a) precipitation (units:  $\text{mm day}^{-1}$ ) and (b) SST (units:  $^{\circ}\text{C}$ )  
531 between the LIA and MCA in the LMR. The gray hatched patterns in part (a) and black dots in  
532 part (b) indicate significant anomalies at the 95% confidence level. The dots in part (a) represent  
533 the reconstructed precipitation/moisture records modified from Chen et al. (2015); the blue (red)  
534 dots denote wetter (drier) conditions in the LIA than in the MCA.

## 535 5 Discussion

536 The features of decadal linkage between moisture/precipitation changes in arid  
537 central Asia and humid monsoonal Asia during the last millennium have been  
538 investigated and the dynamic mechanisms associated with the decadal linkage have  
539 been explored above. Next, the potential linkage on multi-centennial scale implied by  
540 reconstruction is discussed here. Between the LIA and MCA, on multi-centennial  
541 scale, wetter (drier) conditions over arid central Asia and southern China (most of  
542 northern China) were reconstructed in Chen et al. (2015) (Fig. 11a). Besides, the  
543 changes in precipitation between the LIA and the MCA based on the LMR showed  
544 more (less) precipitation over eastern central Asia and southern China (the South



545 Asian monsoon region and most of northern China) (Fig. 11a), consistent with the  
546 reconstructed changes in precipitation/moisture in Chen et al. (2015). These results  
547 suggest a robust centennial linkage of the changes in precipitation/moisture in central  
548 Asia and monsoonal Asia, similar to the decadal precipitation/moisture linkage.

549 The reconstructed changes in the SST between the LIA and MCA showed higher  
550 (lower) SSTs over the central-eastern equatorial Pacific (the western-central parts of  
551 both the subtropical North Pacific and South Pacific) (Fig. 11b). According to the  
552 present study, the IPO-like condition may be the primary cause of the centennial  
553 linkage of changes in precipitation/moisture in central Asia and monsoonal Asia.  
554 However, most current models still cannot reproduce the evolution of the Pacific  
555 Decadal Oscillation (Wang and Miao, 2018). The CESM-LME simulations were also  
556 unable to produce the reconstructed centennial changes in SST between the LIA and  
557 MCA. Therefore, in the present study, we cannot directly obtain the evidence of the  
558 above-mentioned centennial linkage from the CESM-LME results. The failure of  
559 CESM-LME simulations in reproducing the centennial linkage further limits our  
560 understanding of the relative roles and relevant physical processes of the external  
561 forcings and internal variability that shaped the centennial linkage. Thus, further  
562 investigation remains needed.

563

564 **Data availability.** The Last Millennium Reanalysis (LMR) Version 2.1 dataset (Tardif  
565 et al., 2019; Anderson et al., 2019) used in this study are available at  
566 <https://www.atmos.uw.edu/~hakim/LMR/>. The Community Earth System Model-Last



567 Millennium Ensemble (CESM-LME) (Otto-Bliesner et al., 2016) can be founded at  
568 <https://www.cesm.ucar.edu/community-projects/lme>.

569

570 **Author contributions.** TW designed the study; HX analyzed the dataset and plotted  
571 the figures; HX, TW and HW all contributed to writing the manuscript and  
572 interpreting results; Funding was acquired by TW and HX.

573

574 **Competing interests.** The authors declare that they have no conflict of interest.

575

576 **Acknowledgements.** This research has been supported by the National Natural  
577 Science Foundation of China (Grant No. 42221004), the Second Tibetan Plateau  
578 Scientific Expedition and Research Program (STEP, Grant No. 2019QZKK0101), and  
579 the Postgraduate Research and Practice Innovation Program of Jiangsu Province  
580 (KYCX21\_0944).

581

## 582 **References**

583 Aizen, E. M., Aizen, V. B., Melack, J. M., Nakamura, T., and Ohta, T.: Precipitation  
584 and atmospheric circulation patterns at mid-latitudes of Asia, *Int. J. Climatol.*, 21,  
585 535–556, <https://doi.org/10.1002/joc.626>, 2001.

586 Allen, R. G., Pereira, L. S., Raes, D., and Smith, M.: Crop  
587 evapotranspiration-guidelines for computing crop water requirements, Food and  
588 Agriculture Organization of the United Nations Irrigation and Drainage Paper 56,



- 589 1–326, 1998.
- 590 Anderson, D. M., Tardif, R., Horlick, K., Erb, M. P., Hakim, G. J., Noone, D., Perkins,  
591 W. A., and Steig, E.: Additions to the Last Millennium Reanalysis multi-proxy  
592 database, *Data Science Journal*, 18, 1–11, <http://doi.org/10.5334/dsj-2019-002>,  
593 2019.
- 594 Bretherton, C. S., Widmann, M., Dymnikov, V. P., Wallace, J. M., and Bladé I.: The  
595 effective number of spatial degrees of freedom of a time-varying field, *J. Climate*,  
596 12, 1990–2009,  
597 [https://doi.org/10.1175/1520-0442\(1999\)012<1990:tenosd>2.0.co;2](https://doi.org/10.1175/1520-0442(1999)012<1990:tenosd>2.0.co;2), 1999.
- 598 Chen, F., Chen, J., Holmes, J., Boomer, I., Austin, P., Gates, J. B., Wang, N., Brooks,  
599 S. J., and Zhang, J.: Moisture changes over the last millennium in arid central  
600 Asia: a review, synthesis and comparison with monsoon region, *Quaternary Sci.*  
601 *Rev.*, 29, 1055–1068, <https://doi.org/10.1016/j.quascirev.2010.01.005>, 2010.
- 602 Chen, F., Huang, W., Jin, L., Chen, J., and Wang, J.: Spatiotemporal precipitation  
603 variations in the arid Central Asia in the context of global warming, *Sci. China*  
604 *Earth Sci.*, 54, 1812–1821, <https://doi.org/10.1007/s11430-011-4333-8>, 2011.
- 605 Chen, J., Chen, F., Feng, S., Huang, W., Liu, J., and Zhou, A.: Hydroclimatic changes  
606 in China and surroundings during the Medieval Climate Anomaly and Little Ice  
607 Age: spatial patterns and possible mechanisms, *Quaternary Sci. Rev.*, 107, 98–  
608 111, <https://doi.org/10.1016/j.quascirev.2014.10.012>, 2015.
- 609 Chu, C., Yang, X.-Q., Sun, X., Yang, D., Jiang, Y., Feng, T., and Liang, J.: Effect of  
610 the tropical Pacific and Indian Ocean warming since the late 1970s on wintertime





- 611 Northern Hemispheric atmospheric circulation and East Asian climate  
612 interdecadal changes, *Clim. Dynam.*, 50, 3031–3048,  
613 <https://doi.org/10.1007/s00382-017-3790-y>, 2018.
- 614 Cressman, G. P.: Circulations of the west Pacific jet stream, *Mon. Weather Rev.*, 109,  
615 2450–2463, [https://doi.org/10.1175/1520-0493\(1981\)109<2450:cotwpj>2.0.co;2](https://doi.org/10.1175/1520-0493(1981)109<2450:cotwpj>2.0.co;2),  
616 1981.
- 617 Ding, Y.: Advanced synoptic meteorology, China Meteorological Press, Beijing, 2005.
- 618 Ding, Y. and Chan, J. C. L.: The East Asian summer monsoon: an overview, *Meteorol.*  
619 *Atmos. Phys.*, 89, 117–142, <https://doi.org/10.1007/s00703-005-0125-z>, 2005.
- 620 Ding, Y., Wang, Z., and Sun, Y.: Inter-decadal variation of the summer precipitation in  
621 East China and its association with decreasing Asian summer monsoon. Part I:  
622 Observed evidences, *Int. J. Climatol.*, 28, 1139–1161,  
623 <https://doi.org/10.1002/joc.1615>, 2008.
- 624 Dong, B. and Lu, R.: Interdecadal enhancement of the walker circulation over the  
625 Tropical Pacific in the late 1990s, *Adv. Atmos. Sci.*, 30, 247–262,  
626 <https://doi.org/10.1007/s00376-012-2069-9>, 2013.
- 627 Gilman, D. L., Fuglister, F. J., and Mitchell, J. M.: On the power spectrum of “red  
628 noise”, *J. Atmos. Sci.*, 20, 182–184,  
629 [https://doi.org/10.1175/1520-0469\(1963\)020<0182:otpson>2.0.co;2](https://doi.org/10.1175/1520-0469(1963)020<0182:otpson>2.0.co;2), 1963.
- 630 Henley, B. J., Gergis, J., Karoly, D. J., Power, S., Kennedy, J., and Folland, C. K.: A  
631 Tripole Index for the Interdecadal Pacific Oscillation, *Clim. Dynam.*, 45, 3077–  
632 3090, <https://doi.org/10.1007/s00382-015-2525-1>, 2015.



- 633 Huang, J., Ma, J., Guan, X., Li, Y., and He, Y.: Progress in semi-arid climate change  
634 studies in China, *Adv. Atmos. Sci.*, 36, 922–937,  
635 <https://doi.org/10.1007/s00376-018-8200-9>, 2019.
- 636 Huang, W., Chen, F., Feng, S., Chen, J., and Zhang, X.: Interannual precipitation  
637 variations in the mid-latitude Asia and their association with large-scale  
638 atmospheric circulation, *Chinese Sci. Bull.*, 58, 3962–3968,  
639 <https://doi.org/10.1007/s11434-013-5970-4>, 2013.
- 640 Huang, W., Chen, J., Zhang, X., Feng, S., and Chen, F.: Definition of the core zone of  
641 the “westerlies-dominated climatic regime”, and its controlling factors during the  
642 instrumental period, *Sci. China Earth Sci.*, 58, 676–684,  
643 <https://doi.org/10.1007/s11430-015-5057-y>, 2015.
- 644 Hurrell, J. W., Holland, M. M., Gent, P. R., Ghan, S., Kay, J. E., Kushner, P. J.,  
645 Lamarque, J.-F., Large, W. G., Lawrence, D., Lindsay, K., Lipscomb, W. H.,  
646 Long, M. C., Mahowald, N., Marsh, D. R., Neale, R. B., Rasch, P., Vavrus, S.,  
647 Vertenstein, M., Bader, D., Collins, W. D., Hack, J. J., Kiehl, J., and Marshall, S.:  
648 The Community Earth System Model: A framework for collaborative research, *B.*  
649 *Am. Meteorol. Soc.*, 94, 1339–1360, <https://doi.org/10.1175/bams-d-12-00121.1>,  
650 2013.
- 651 Jiang, D., Su, M., Wei, R., and Bao, L.: Variation and projection of drought and wet  
652 conditions in Xinjiang, *Chinese Journal of Atmospheric Sciences*, 33, 90–98,  
653 <https://doi.org/10.3878/j.issn.1006-9895.2009.01.08>, 2009.
- 654 Jiang, J., Zhou, T., Chen, X., and Wu, B.: Central Asian precipitation shaped by the



- 655 tropical Pacific Decadal Variability and the Atlantic Multidecadal Variability, *J.*  
656 *Climate*, 34, 7541–7553, <https://doi.org/10.1175/jcli-d-20-0905.1>, 2021.
- 657 Jin, C., Liu, J., Wang, B., Yan, M., and Ning, L.: Decadal variations of the East Asian  
658 summer monsoon forced by the 11-year insolation cycle, *J. Climate*, 32, 2735–  
659 2745, <https://doi.org/10.1175/jcli-d-18-0288.1>, 2019.
- 660 Krishnamurthy, L. and Krishnamurthy, V.: Influence of PDO on South Asian summer  
661 monsoon and monsoon–ENSO relation, *Clim. Dynam.*, 42, 2397–2410,  
662 <https://doi.org/10.1007/s00382-013-1856-z>, 2014.
- 663 Li, B., Li, Y., Chen, Y., Zhang, B., and Shi, X.: Recent fall Eurasian cooling linked to  
664 North Pacific sea surface temperatures and a strengthening Siberian high, *Nat.*  
665 *Commun.*, 11, 5202, <https://doi.org/10.1038/s41467-020-19014-2>, 2020.
- 666 Li, G., Gao, C., Lu, B., and Chen, H.: Inter-annual variability of spring precipitation  
667 over the Indo-China Peninsula and its asymmetric relationship with El  
668 Niño–Southern Oscillation, *Clim. Dynam.*, 56, 2651–2665,  
669 <https://doi.org/10.1007/s00382-020-05609-4>, 2021.
- 670 Li, T., Wang, Y., Wang, B., Ting, M., Ding, Y., Sun, Y., He, C., and Yang, G.:  
671 Distinctive South and East Asian monsoon circulation responses to global  
672 warming, *Sci. Bull.*, 67, 762–770, <https://doi.org/10.1016/j.scib.2021.12.001>,  
673 2022.
- 674 Middleton, N. J. and Thomas, D. S. G.: *World atlas of desertification*, 2nd edn,  
675 Edward Arnold, London, The United Kingdom, 1997.
- 676 Mishra, V. and Aadhar, S.: Famines and likelihood of consecutive megadroughts in



- 677 India, *npj Clim. Atmos. Sci.*, 4, 59, <https://doi.org/10.1038/s41612-021-00219-1>,  
678 2021.
- 679 Monteith, J. L.: Evaporation and environment, *Symposia of the Society for*  
680 *Experimental Biology*, 19, 205–234, 1965.
- 681 Ning, L., Chen, K., Liu, J., Liu, Z., Yan, M., Sun, W., Jin, C., and Shi, Z.: How do  
682 volcanic eruptions influence decadal megadroughts over eastern China?, *J.*  
683 *Climate*, 33, 8195–8207, <https://doi.org/10.1175/JCLI-D-19-0394.1>, 2020.
- 684 Otto-Bliesner, B. L., Brady, E. C., Fasullo, J., Jahn, A., Landrum, L., Stevenson, S.,  
685 Rosenbloom, N., Mai, A., and Strand, G.: Climate variability and change since  
686 850 CE: An ensemble approach with the Community Earth System Model, *B.*  
687 *Am. Meteorol. Soc.*, 97, 735–754, <https://doi.org/10.1175/bams-d-14-00233.1>,  
688 2016.
- 689 PAGES2k Consortium: A global multiproxy database for temperature reconstructions  
690 of the Common Era, *Sci. Data*, 4, 170088, <https://doi.org/10.1038/sdata.2017.88>,  
691 2017.
- 692 Penman, H. L.: Natural evaporation from open water, bare soil and grass, *Proc. R. Soc.*  
693 *Lond. A*, 193, 120–145, <https://doi.org/10.1098/rspa.1948.0037>, 1948.
- 694 Power, S., Casey, T., Folland, C., Colman, A., and Mehta, V.: Inter-decadal  
695 modulation of the impact of ENSO on Australia, *Clim. Dynam.*, 15, 319–324,  
696 <https://doi.org/10.1007/s003820050284>, 1999.
- 697 Qin, M., Dai, A., Li, D., and Hua, W.: Understanding the inter-decadal variability of  
698 autumn precipitation over North Central China using model simulations, *Int. J.*



- 699           Climatol., 40, 874–886, <https://doi.org/10.1002/joc.6245>, 2020.
- 700   Qin, M., Li, D., Dai, A., Hua, W., and Ma, H.: The influence of the Pacific Decadal  
701           Oscillation on North Central China precipitation during boreal autumn, *Int. J.*  
702           *Climatol.*, 38, e821–e831, <https://doi.org/10.1002/joc.5410>, 2018.
- 703   Shi, J., Yan, Q., Jiang, D., Min, J., and Jiang, Y.: Precipitation variation over eastern  
704           China and arid central Asia during the past millennium and its possible  
705           mechanism: Perspectives from PMIP3 experiments, *J. Geophys. Res.-Atmos.*,  
706           121, 11,989–12,004, <https://doi.org/10.1002/2016JD025126>, 2016.
- 707   Shi, Y., Shen, Y., Kang, E., Li, D., Ding, Y., Zhang, G., and Hu, R.: Recent and Future  
708           climate change in Northwest China, *Climatic Change*, 80, 379–393,  
709           <https://doi.org/10.1007/s10584-006-9121-7>, 2007.
- 710   Tardif, R., Hakim, G. J., Perkins, W. A., Horlick, K. A., Erb, M. P., Emile-Geay, J.,  
711           Anderson, D. M., Steig, E. J., and Noone, D.: Last Millennium Reanalysis with  
712           an expanded proxy database and seasonal proxy modeling, *Clim. Past*, 15, 1251–  
713           1273, <https://doi.org/10.5194/cp-15-1251-2019>, 2019.
- 714   Turner, A. G. and Annamalai, H.: Climate change and the South Asian summer  
715           monsoon, *Nat. Clim. Change*, 2, 587–595, <https://doi.org/10.1038/nclimate1495>,  
716           2012.
- 717   Wang, H. J.: The weakening of the Asian monsoon circulation after the end of 1970's,  
718           *Adv. Atmos. Sci.*, 18, 376–386, <https://doi.org/10.1007/BF02919316>, 2001.
- 719   Wang, T. and Miao, J. P.: Twentieth-century Pacific Decadal Oscillation simulated by  
720           CMIP5 coupled models, *Atmos. Ocean Sci. Lett.*, 11, 94–101,



- 721 <https://doi.org/10.1080/16742834.2017.1381548>, 2018.
- 722 Wang, T., Wang, H. J., Otter & O. H., Gao, Y. Q., Suo, L. L., Furevik, T., and Yu, L.:  
723 Anthropogenic agent implicated as a prime driver of shift in precipitation in  
724 eastern China in the late 1970s, *Atmos. Chem. Phys.*, 13, 12433–12450,  
725 <https://doi.org/10.5194/acp-13-12433-2013>, 2013.
- 726 Wang, T., Xu, H., Jiang, D., and Yao, J.: Mechanisms of reduced mid-Holocene  
727 precipitation in arid Central Asia as simulated by PMIP3/4 models, *J. Geophys.*  
728 *Res.-Atmos.*, 127, e2021JD036153, <https://doi.org/10.1029/2021JD036153>,  
729 2022.
- 730 Webster, P. J. and Yang, S.: Monsoon and ENSO: Selectively interactive systems, *Q. J.*  
731 *Roy. Meteor. Soc.*, 118, 877–926, <https://doi.org/10.1002/qj.49711850705>, 1992.
- 732 Xu, H., Wang, T., Wang, H., Miao, J., Chen, J., and Chen, S.: The PMIP3 simulated  
733 climate changes over arid Central Asia during the mid-Holocene and last glacial  
734 maximum, *Acta Geol. Sin.-Engl.*, 94, 725–742,  
735 <https://doi.org/10.1111/1755-6724.14542>, 2020.
- 736 Xue, J., Ning, L., Liu, Z., Qin, Y., Chen, K., Yan, M., Liu, J., Wang, L., and Li, C.:  
737 The combined influences of solar radiation and PDO on precipitation over  
738 eastern China during the last millennium, *Clim. Dynam.*, 60, 1137–1150,  
739 <https://doi.org/10.1007/s00382-022-06372-4>, 2023.
- 740 Zhang, Y. and Huang, D.: Has the East Asian westerly jet experienced a poleward  
741 displacement in recent decades?, *Adv. Atmos. Sci.*, 28, 1259–1265,  
742 <https://doi.org/10.1007/s00376-011-9185-9>, 2011.



- 743 Zhao, P., Yang, S., and Yu, R.: Long-term changes in rainfall over eastern China and  
744 large-scale atmospheric circulation associated with recent global warming, *J.*  
745 *Climate*, 23, 1544–1562, <https://doi.org/10.1175/2009jcli2660.1>, 2010.
- 746 Zhao, X., Dong, B., and Lu, R.: Interdecadal weakening of the cross-equatorial flows  
747 over the Maritime Continent during the boreal summer in the mid-1990s: drivers  
748 and physical processes, *Clim. Dynam.*, 57, 55–72,  
749 <https://doi.org/10.1007/s00382-021-05692-1>, 2021.
- 750 Zhu, J., Zhao, K., Wang, Y., Cui, Y., Liang, Y., Cheng, H., Edwards, R. L., Kong, X.,  
751 Shao, X., Chen, S., and Pang, L.: Decadal modulation of East Asian summer  
752 monsoon variations by external forcing and internal variability, *Quaternary Sci.*  
753 *Rev.*, 293, 107720, <https://doi.org/10.1016/j.quascirev.2022.107720>, 2022.
- 754 Zhu, Y., Wang, H., Ma, J., Wang, T., and Sun, J.: Contribution of the phase transition  
755 of Pacific Decadal Oscillation to the late 1990s' shift in East China summer  
756 rainfall, *J. Geophys. Res.-Atmos.*, 120, 8817–8827,  
757 <https://doi.org/10.1002/2015JD023545>, 2015.